Nanoscale

Accepted Manuscript

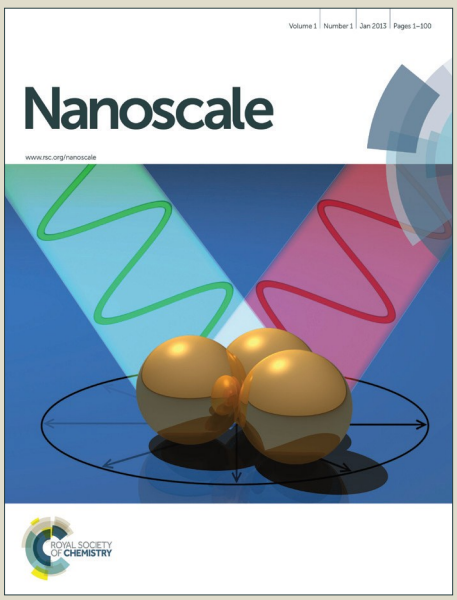

ROYAL SOCIETY OF CHEMISTRY

www.rsc.org/nanoscale

Thermal Conductivity of Electrospun Polyethylene Nanofibers

Jian Ma,[1,2,*] Qian Zhang,[1,*] Anthony Mayo,[3] Zhonghua Ni,[2] Hong Yi,[2] Yunfei Chen,[2] Richard Mu,[3,4] Leon Bellan,[1] and Deyu Li[1,a]

[1]*Department of Mechanical Engineering, Vanderbilt University, Nashville, TN, 37235, United States.*

[2]*Jiangsu Key Laboratory for Design and manufacture of Micro-Nano Biomedical Instruments, School of Mechanical Engineering, Southeast University, Nanjing, 100084, China.*

[3]*Department of Physics, Fisk University, Nashville, TN, 37208, United States.*

[4]*TIGER Institute, Tennessee State University, Nashville, TN, 37209, United States.*

[*]*These authors contribute to the paper equally*

[a]*E-mail: deyu.li@vanderbilt.edu*

Abstract

We report on the structure-thermal transport property relation of individual polyethylene nanofibers fabricated by electrospinning with different deposition parameters. Measurement results show that the nanofiber thermal conductivity depends on the electric field used in the electrospinning process, with a general trend of higher thermal conductivity for fibers prepared with stronger electric field. Nanofibers produced at a 45 kV electrospinning voltage and a 150 mm needle-collector distance could have a thermal conductivity of up to 9.3 W/m-K, over 20 times higher than the typical bulk value. Micro-Raman characterization suggests that the enhanced thermal conductivity is due to the highly oriented polymer chains and enhanced crystallinity in the electrospun nanofibers.

Introduction

Electrospun nanofibers and nanofibrous mats have been extensively tested as scaffolds for cell culture,[1] light sources,[2] waveguides,[3, 4] transistors,[5-7] gas sensors,[8] zeptomole scale reactors,[9] fuel cell proton exchange membranes,[10, 11] templates for nanopatterning,[12, 13]as well as filters to trap minute particles without significantly impeding air flow.[13, 14] To date, most electrospun nanofibers are made of polymers, one of the most dominant categories of materials in modern civilization, with innumerable applications in industry and everyday life. As the small fiber size and high surface area of electrospun mats are attractive for many applications, systems for electrospinning at a commercial scale (e.g. Nanospider™ by Elmarco and Nanospinner416 by Inovenso) are already available, and a wide range of products containing electrospun nanofibers are currently for sale, illustrating the scalability of the manufacturing process.

One important issue with polymeric materials is their low thermal conductivity, which limits their use in many applications. Bulk polymers usually have extremely low thermal conductivity on the order of 0.1 W/m-K. In response to demands for fast heat dissipation in various applications such as flexible electronics,[15] photovoltaic energy conversion,[16] and advanced structural materials mounted with high power electronics,[17] tremendous efforts have been made to enhance the thermal conductivity of polymers, but only with limited success. The low thermal conductivity of polymers comes from their structure, with numerous molecular chains coiled up and entangled together. However, it has been found that commercially available polymer microfibers with highly aligned polymer chains can have much higher thermal conductivity, up to 20 W/m-K, as well as a Young's modulus much higher than typical bulk values.[18] More astonishingly, recent molecular dynamics simulations[19, 20] predicted a thermal conductivity as high as 350 W/m-K for simple polymer chains of polyethylene (PE),[21] which has been supported by subsequent experimental measurements of mechanically-drawn PE nanofibers, yielding a thermal conductivity of ~100 W/m-K.[22] Using a time-domain thermoreflectance (TDTR) method, Wang et al. measured thermal conductivities of several commercially available high-modulus polymer fibers.[18] Their results indicate that liquid crystalline p-phenylene benzobisoxazole (PBO) fibers have the highest room temperature thermal conductivity of ~20 W/m-K, surpassing the

conductivity of commercially available highly crystalline PE. One more interesting result by Singh et al. shows that pure polythiophene nanofibers can have a thermal conductivity up to ~4.4 W/m-K (more than 20 times higher than the bulk polymer value) while remaining amorphous.[23] These pioneering studies strongly suggest that the thermal conductivity of a polymeric material is closely related to its microstructure, especially molecular orientation.

Electrospinning can produce well-aligned polymer nanofiber arrays with ordered molecular chains inside each fiber, pointing to the possibility of large-scale manufacturing of nanofibers with high thermal conductivity. However, there are only very limited studies on the thermal conductivity of individual electrospun nanofibers. A recent study showed that the thermal conductivity of single Nylon-11 electrospun fibers could be as high as 1.6 W/m-K, nearly one order of magnitude higher than the typical Nylon-11 bulk value of around 0.2 W/m-K.[24] However, all the electrospun nanofibers studied in the above-mentioned report were produced with a relatively low voltage of 6-7 kV, with no attempt made to push the limit of the thermal conductivity by changing the processing conditions. One more study by Canetta et al. measured the thermal conductivity of individual polystyrene nanofibers which were electrospun at 7-10 kV.[25] The thermal conductivity of the measured nanofibers ranges from 6.6 and 14.4 W/m-K, a significant increase from the typical bulk values for polystyrene. The increased thermal conductivity of electrospun nanofibers has been attributed to the aligned molecular chains resulted from the high strain rates within the electrospinning jets.

In this paper, we report on measurements of the thermal conductivity of electrospun PE nanofibers prepared under different electric fields to explore the effects of electric field intensity on the molecular alignment and resulted thermal conductivity. To correlate the relation between structure and thermal conductivity, we conducted micro-Raman characterization on individual nanofibers. We choose to study PE nanofibers because of the simple molecular structure, and the promising results obtained from ultra-drawn PE nanofibers.

Experimental Approach

Electrospinning has become a widely used technique to form nanofibers from a variety of materials with diameters ranging from tens of nanometers to a few microns. In a typical

electrospinning process, a solution of polymer molecules dissolved in solvent is supplied to the tip of a sharp conductor, such as a syringe needle. A high voltage is applied between the conductor and a grounded collector. Under the influence of the strong electric field, the polymer solution forms a cone (often called a Taylor cone), from which a jet is accelerated towards the grounded collector. This jet is a strong elongational flow, and becomes thinner as it approaches the collector. Due to the very large surface area-to-volume ratio of the jet, the solvent evaporates quickly, leaving a solid fiber that is deposited on the collecting surface. It is worth noting that a "whipping" instability often results in a jet path that is longer than the tip-collector distance, and causes the fiber deposition to move chaotically over the collector. This could lead to a significant variation in the structure and property of the nanofibers from a single deposition.

To electrospin PE, we first dissolved ultrahigh molecular weight PE powder (molecular weight $3\sim6\times10^6$) in p-xylene and cyclohexanone mixture solution (all materials from Sigma-Aldrich, Inc.). P-xylene is a well-known solvent for PE.[26-28] However, the electrical conductivity of p-xylene is very low, with a value of ~3 pS/m. In addition, the dielectric constant of p-xylene is only about 2.4. As such, to boost the electrical conductivity and dielectric constant of the solution, cyclohexanone was added to p-xylene at a 1:1 weight ratio. To prepare the solution, the solvent mixture was first heated to 120 ^{o}C and then 0.1 wt% of PE powder was added. The PE solution was stirred at 120 ^{o}C till the powder was completely dissolved, and then the solution was poured into a glass syringe that was preheated to 120 ^{o}C. The glass syringe was placed on a syringe pump with a 20-gauge metal needle attached to the end. To keep the temperature of the PE solution at ~120 ^{o}C, an infrared quartz radiant heater (Optimus HT-511) was placed on one lateral side of the syringe and needle, as shown in the schematic of the set-up in Fig. 1a. The syringe pump was set to generate a constant flow rate of 200 μl/min.

It is well known that in PE powders, some PE molecular chains are folded locally in the form of small crystallites, usually termed as "lamellae",[26, 29] while other molecular chains are randomly distributed (Fig. 1b). When the PE powder completely dissolved in the solvent, both lamellae and entangled molecular chains dissolved in a random orientation (Fig. 1c). During the electrospinning process, the random molecular chains will be aligned in an order

fashion as shown in Fig. 1d. The electrospinning deposition was performed at a wide scope of voltages ranging from 9 kV to 52 kV, with a fixed distance of 150 mm between the tip of the spinneret and the collector. The fibers were collected on small pieces of silicon wafers for examination by Raman and on PDMS membranes for transfer to thermal conductivity measurement devices. The high voltage was supplied by an EMCO DX250 DC-DC converter. It is worth noting that even though the manufacture specified voltage limit is up to only 25 kV, we successfully extracted up to 52 kV as measured with a BK precision high voltage digital multimeter probe (BK PR-28A).

The thermal measurement of individual nanofibers was conducted with a microdevice designed to measure the thermal conductivity of various nanowires, nanotubes, and nanoribbons.[30, 31] With the help of a home built micromanipulator, the as-deposited fibers, after being collected on a piece of PDMS (Fig. 2a), were cut and transferred to the thermal conductivity measurement device (Fig. 2b). The thermal conductivity of each fiber was measured in a temperatures range from 100 K to 320 K. The measurement was conducted in a cryostat with a high vacuum ($<2\times10^{-6}$ mbar) to minimize convective heat transfer. To reduce the effects from radiation heat loss, the sample is separated from the vacuum shroud by two radiation shields, including one directly mounted on the sample holder (high temperature stage).[32] For measurement of small thermal conductance samples (~ nW/K), the background signal will be a significant portion of the total measured thermal conductance. Thus a blank device with the same membrane gap (~6 um) was characterized to extract the background heat transfer as a result of radiation and residual air convection. All devices used in the measurement were fabricated using the same fabrication procedure and of the same nominal geometry. Thus, it is reasonable to assume the same background heat transfer rate,[33] and all thermal conductivity results presented here were calculated based on thermal conductance after subtraction of the background heat transfer. Post the thermal measurement, the geometrical information of the measured fiber was extracted using scanning electron microscopy (SEM) (Fig. 2c).

No contact treatment was done to minimize the contact thermal resistance between the fiber and the suspended membranes. Thus, the reported results represent a lower bound for the true thermal conductivity. It is worth noting that for all samples, the contact length

between the nanofiber and the suspended membranes is quite long, and the nanofibers stick well to the suspended membrane. These facts, together with that the measured thermal conductivity is still relatively low, which corresponds to a relatively large fiber resistance, suggests that the contribution from the contact thermal resistance is small compared with the resistance of the fiber. In Zhong et al. study,[24] they have proven that the contact thermal resistance was an insignificant portion of the total measured resistance. We evaluated the thermal contact resistance using their theoretical model, which showed that the contact resistance contributed less than 5% of the total measured thermal resistance.

Structural characterization techniques such as X-ray diffraction (XRD) and infrared spectroscopy are usually used to study electrospun nanofibers; however, these measurements are typically performed on large bundles in order to achieve acceptable signal-to-noise ratios. Raman spectroscopy offers many advantages for the study of individual fibers, as it provides molecular level information about conformation, interactions, and crystallinity, yet only requires a small sample volume. Over the past two decades, Raman spectroscopy has been widely used to characterize PE and the corresponding vibrational modes of the Raman bands are well known.[34-40] More recently, Bellan and Craighead proposed using micro-Raman to characterize the molecular orientation within single nylon-6 electrospun nanofibers.[41] The internal normal modes between 1000-1600 cm^{-1} are commonly used to study morphological structure and can be divided in three vibrational regimes:[42] the C-C stretching between 1000 and 1200 cm^{-1}, which are sensitive to molecular orientation, stress and conformation; the $-CH_2-$ twisting vibrations around 1295 cm^{-1}, which can be used as an internal standard; and the $-CH_2-$ bending modes between 1400 and 1470 cm^{-1}, which are sensitive to chain packing (the 1416 cm^{-1} band is assigned to orthorhombic crystallinity). The assignment of bands in the Raman spectrum of PE is given in details in Table 1.

In this study, we use micro-Raman spectroscopy to evaluate the molecular chain orientation and crystallinity of individual electrospun PE nanofibers. The Raman spectra of the PE nanofibers were collected from individual free-standing fibers suspended over Si trenches using a Horiba LabRam HR800 system. The Raman characterization was conducted at room temperature using 10 mW of radiation at a wavelength of 532 nm (LaserQuantum ventus 532) (Fig. 2d). The spectra were accumulated for 1 minute and

taken with a slit width equivalent to 1.5 cm^{-1} resolution. For the purpose of microstructural characterization, it is necessary to first verify that during the characterization process with micro-Raman spectroscopy, heating from the laser would not significantly alter the structure of the nanofiber sample. Fig. 3 shows three Raman spectra taken at the same position of two nanofibers electrospun at different voltages with a laser power of 10 mW. Each spectra was accumulated for 1 minute (Note that to further minimize the damage from the Raman characterization, a laser power of 0.01 mW was used during the alignment process). These three Raman spectra essentially overlap with each other, suggesting marginal microstructural alteration while undergoing Raman characterization. We subsequently used this technique to characterize the ultra-high molecular weight PE powder and nanofibers prepared at various voltages (Fig. 4). The Raman spectra for fibers fabricated at higher electrospinning voltages, which are very different from the PE power as shown in Fig. 4, further indicate that the laser power in the Raman characterization will not drastically alter the structure of the fiber because otherwise all spectra should be similar to that of the PE powder.

Results and Discussion

Fig. 5a shows the room temperature thermal conductivity of electrospun nanofibers at different electrospinning voltages. As mentioned previously, the whipping instability typically seen in an electrospinning jet can lead to variations in the deposited fibers during a given electrospinning process. As such, the measured thermal conductivities for fibers fabricated under the same electrospinning voltage can vary significantly. However, even with this variation, there is a clear trend of enhanced thermal conductivity as the electrospinning voltage increases. In fact, even at a relatively low voltage of 9 kV, the thermal conductivity of the measured PE nanofiber is about 0.8 W/m-K, about two folds of the bulk value for high density PE (0.4 W/m-K).[43]

It is widely accepted that stretching crystalline polymer films and fibers can modify the crystalline structure or induce crystal transition in their structures. During the electrospinning process, the PE molecular chains experience strong elongational forces, which give rise to PE fibers with a high degree of molecular orientation and a better crystallinity. In general, the higher the applied electrospinning voltage is, the stronger the

elongational force will be, and as a result, fibers will be composed of more aligned molecules and of higher crystallinity. Therefore, it is very reasonable to observe higher thermal conductivity values as the electrospinning voltage is increased. In fact, the highest thermal conductivity measured at each electrospinning voltage increases almost linearly with the voltage.

The highest thermal conductivity we measured is 9.3 W/m-K, which is obtained with an electrospinning voltage of 45 kV. Even though we expected that higher thermal conductivity could be achieved at 52 kV, the highest value measured is only 7.8 W/m-K from the two fibers prepared with 52 kV, which could be due to a few reasons. First, due to the limitations of our instrumentation, 52 kV was the highest voltage we could achieve, with problems such as strong arcing occurring at this voltage. Secondly, there is a trade-off between the stronger electrical field and shorter flight time in the electrospinning process. Olubayode et al. found that there exists an optimum voltage to achieve the highest degree of crystallinity in electrospun Poly (L-lactic acid) (PLLA).[44] At electrospinning voltages higher or lower than the optimum voltage, the degree of crystallinity would drop to a lower level. This is because while a higher electrospinning voltage exerts a stronger stretching force, the flight time is shorter, thus leaving less time for crystalline structure formation. No matter what the reason is, it is worth exploring how to optimize the fabrication set-up to extend the applied electrospinning voltage to higher values and observe whether even larger values of thermal conductivity can be achieved.

We further verified that the thermal conductivity enhancement is indeed due to the structural change using Raman spectroscopy. A semi-quantitative approach to determine the molecular orientation in PE, using the ratio of the 1130 cm^{-1} and 1060 cm^{-1} Raman bands, has been reported.[40, 42, 45] These two bands have different vibrational symmetries. The 1130 cm^{-1} Raman band is thought to arise from the C-C symmetric stretching of the all-trans PE chain segments while the 1060 cm^{-1} band is due to the two degenerated C-C antisymmetric stretching. If the molecules are oriented in a preferred direction, the 1130 cm^{-1} band has been reported to become stronger with respect to the 1060 cm^{-1} band. As shown in Fig. 4, as the electrospinning voltage increases, the intensity ratio of the 1130 cm^{-1} and 1060 cm^{-1} bands becomes significantly larger, indicating that the molecular chains in the

fibers are better aligned.

To further investigate molecular orientation in the PE nanofibers, we measured the Raman spectra on multiple samples prepared at different voltages. Fig. 5b shows the correlation between the 1130/1060 band intensity ratio and the electrospinning voltage. This ratio for ultra-high molecular weight PE powders is about 1.16. For nanofibers fabricated with relatively low electrospinning voltages, this ratio is close to the powder value. As the voltage gets larger, there is a clear increasing trend for the obtained 1130/1060 ratio, suggesting that the PE chains experience stronger elongational force at higher electrospinning voltage, which results in fibers with a higher degree of molecular orientation.

To further observe the temperature dependence of the PE nanofibers, Fig. 5c shows the thermal conductivity of PE fibers fabricated from 9 kV to 45 kV at temperatures ranging from 100 to 320 K. Note that the thermal conductivity of the nanofiber sample with the highest measured values at each electrospinning voltage was plotted in Fig. 5c. These data suggest that while the thermal conductivity for fibers prepared at low voltages remains nearly the same or only increases marginally with temperature in the whole temperature range, the thermal conductivity of fibers prepared at higher electrospinning voltages increases clearly from 100 K to 250-270 K. Beyond 250-270 K, the thermal conductivity starts to drop as temperature increases further, which is a signature of phonon UmKlapp scattering.[18, 46] The different temperature dependence indicates that as the electrospinning voltage increases, the crystallinity level increases, leading to UmKlapp scattering, which is a signature of phonon transport in crystalline materials.

The crystalline phase of PE is primarily orthorhombic, although it has been suggested that monoclinic structures coexist under certain conditions, including uniaxial deformation.[39, 40, 42, 47] The band at 1416 cm^{-1} has been unanimously assigned to the orthorhombic crystalline phase while attribution of other bands exclusively to the amorphous or crystalline phase is still a matter of debate. According to the Raman spectra of PE nanofibers (Fig. 4), it is clear that the 1416 cm^{-1} band, or the orthorhombic crystallinity, becomes stronger as the voltage increases. To more quantitatively determine the fraction of the orthorhombic crystalline phase, amorphous phase and intermediate phase, we utilize the curve fitting algorithm provided in the LapSpec software package. Following Strobl and Hagedorn,[34] the

orthorhombic crystallinities can be calculated according to the band areas ratio of $I_{1416}/I_{1295+1305}$:

$$\%\text{orthorhombic crystallinity} = (I_{1416}/I_{1295+1305})\times(100/0.45), \quad (1)$$

where I_{1416} is the areas underneath the Raman bands at 1416 cm^{-1}, $I_{1295+1305}$ is the area underneath the internal standard band group. Note that this formula could only be used to calculate the Raman crystallinity of isotropic sample. For highly oriented systems, Lagaron et al. suggested that the influence of the molecular orientation should be removed or the Strobl and Hagedorn formula cannot be directly applied.[42] They provided a modified formula with a correction factor, *K*, for additional orientation effects.

$$\%\text{orthorhombic crystallinity} = (I_{1416}/I_{1295+1305})\times(100/0.45)\times K. \quad (2)$$

As shown in Fig. 5d, the band area ratio $I_{1416}/I_{1295+1305}$ increases with the electrospinning voltage, suggesting that the PE nanofibers produced at higher voltages have a larger volume fraction of the orthorhombic crystalline phase. The band area ratio displays a wide distribution for any given voltage, which is again because of the 'whipping instability' in the fiber deposition process. However, even with significant variations, the trend can still be clearly seen.

One more observation is that with higher electrospinning voltage, the factor-group split bands of the orthorhombic band (1440 cm^{-1} and 1460 cm^{-1}) decreases (Fig. 4). In fact, at 52 kV, the 1416 cm^{-1} factor-group split band almost disappears. Lagaron et al. have observed that the presence of monoclinic or triclinic structures would influence the 1416 cm^{-1} factor-group splitting bands.[40, 42] They claimed that the spectral changes are due to not only the presence of the monoclinic phase but also the creation of an ill-defined orthorhombic crystalline structure with dislocations and disrupted crystals formed by the cold-drawing process, as a result of molecules being pulled through the crystals.

While we observed a strong dependence of the thermal conductivity on the electrospinning voltage, we did not find a clear relation between the thermal conductivity and diameter (Fig. 6a). In the study of Zhong et al., the thermal conductivities of electrospun Nylon-11 fibers prepared at relatively low voltages (6-7 kV) show a size dependence with higher thermal conductivities for smaller fibers, which is possibly due to better chain alignment in smaller fibers.[24] In fact, in Fig. 6a, three of the four samples synthesized at the

same voltage exhibit an increase in thermal conductivity with decreasing diameter, with one being an outlier. However, overall we did not find a consistent diameter dependence, especially as the fabrication voltage varies. One difference in their study is that their fibers span a large diameter range and all fibers are prepared with a relatively low and consistent electrospinning voltage, where the 'whipping instability' might not be as strong. In our case, however, the fibers are of relatively smaller diameters and fabricated at higher voltage range. The higher voltage leads to stronger 'whipping instability', and hence large variations in the actual electric field the jet experiences during the fabrication process, which likely eliminate any dependence on the fiber diameter.

In Fig. 6b, we compare our thermal conductivity data with other published data for PE including a commercial high crystalline PE nanofiber (Dyneema and Spectra 900) and bulk thermal conductivity of PE. The selected electrospun fiber, fabricated at 45 kV, demonstrated a peak value of 9.3 W/m-K around 270 K, and then the thermal conductivity drops with temperature and reaches a value of 8.7 W/m-K at 320 K. The peak temperature is, however, much higher than that of the commercial high modulus PE fiber, which has a broad peak centering at ~100 K. The difference in the peak temperature suggests that the crystallinity level of the electrospun fiber is still lower than the Dyneema and Spectra 900 fiber, with abundant amorphous phases and strong inter-chain scattering at low temperatures. However, the anharmonicity is strong enough to show its signature at a higher temperature.

One interesting effect we found during the measurements is that annealing, caused by an electron beam, could drastically alter the nanofiber structure and its thermal conductivity.[48] Fig. 6b also plots the thermal conductivity of the same fiber after it was exposed to scanning electron microscopy (SEM) imaging, which indicates that the thermal conductivity drops to that of bulk amorphous PE. There is no discernable peak in the measured thermal conductivity after the SEM, either.

To further clarify the electron beam annealing effects, we prepared additional samples and compared the measured thermal conductivity before and after SEM. We found that the electron beam can indeed lead to significant morphological change. Fig. 7a and 7b give the length of the same fiber sample prepared with a 45 kV electrospinning voltage at the beginning and the end of an SEM imaging process of ~1 min with an acceleration voltage of

5 kV, which indicates that the gap between the two suspended membranes shrinks from 6.6 μm to 5.8 μm. Note that this observation also suggests that the fiber adheres to the suspended membranes well and the interaction force is strong enough to prevent sliding of the fiber with respect to the membranes; instead, the fiber pulls the two membranes closer to each other. As to the thermal conductivity of the fiber prior to and after the SEM imaging, the value changes dramatically, dropping from a room temperature value of ~5 W/m-K to 0.4 W/m-K, as shown in Fig. 7c. In order to accurately measure the diameter of the fiber, multiple micrographs were taken quickly to monitor the dimension change during the SEM imaging. We assume that the volume of the suspended segment does not change and the original diameter was calculated using the formula $d_{original} = \sqrt{d_{final}^2 \times l_{final} / l_{original}}$. Here $d_{original}$ and $l_{original}$ are the initial diameter and length of the fiber prior to the SEM imaging and d_{final} and l_{final} are the diameter and length of the fiber post the SEM imaging.

As mentioned before, larger 1130/1060 band intensity ratio for PE fibers deposited at higher voltages corresponds to better aligned molecule chains, and larger $I_{1416}/I_{1295+1305}$ band area ratio indicates a higher orthorhombic crystallinity level. Fig. 7d shows the difference in Raman spectra of the same PE fiber prepared at 30 kV before and after the SEM imaging. Before the electron beam exposure the 1130/1060 ratio was 1.87, while after the SEM it dropped to 0.49, even smaller than the corresponding value of PE powder (1.16). In addition, prior to the SEM imaging, the intensity of the orthorhombic band at 1416 cm^{-1} was very strong but it almost disappeared post the SEM. All these data indicate that the focused electron beam remarkably altered the degree of orientation of the PE fiber and reduced the fraction of the orthorhombic crystallinity, leading to much lower thermal conductivity.

In the electrospinning process, we found that the solvent could be trapped inside the fiber at relatively high solution flow rates. Fig. 8a shows the Raman spectra of PE nanofibers electrospun at various voltages with an 18 G needle and a 500 μl/min solution volume flow rate (Note that this is different from what we used for the preparation of fiber samples in thermal conductivity measurements, where conditions were tuned to leave minimum solvent residue in the fiber). It can be seen that the Raman spectra of the PE nanofibers prepared with a low voltage is essentially the same as those of the PE powder, while the intensity of

the solvent peaks becomes stronger as the electrospinning voltage increases. This suggests that at higher voltage, the jet flies faster, leaving less time for the solvent to evaporate. As a result, with increased electrospinning voltage, it becomes easier for solvent to be trapped inside the fiber. However, it was found that after storing the deposited fibers in a vacuum of 10^{-3} mbar overnight, the Raman peaks corresponding to the presence of solvent disappeared, suggesting we could effectively remove the residual solvent (Fig. 8b). This also guarantees that no complication from the solvent exists in our measurements because it is conducted under a much higher vacuum ($<2\times10^{-6}$ mbar).

Summary

In this study we explore the relation among the electrospinning voltage, resulted nanofiber structure, and the corresponding thermal conductivity. Results show that electrospun PE nanofibers exhibit thermal conductivity that can be significantly higher than bulk values (~0.4 W/m-K), with the highest value measured as 9.3 W/m-K. This thermal conductivity enhancement is due to the higher degree of molecule orientation and enhanced level of crystallinity, as evidenced by the micro-Raman spectroscopy characterization. A general trend of higher thermal conductivity with larger electrospinning voltage was observed (up to 45 KV); however, it is also found that the thermal conductivity for fibers prepared with the same voltage could vary significantly, likely due to the 'whipping instability' in the electrospinning process. Due to the limitations of our current instrumentation, the maximum electrospinning voltage achieved was 52 kV. With an electrospinning system capable of operating at higher voltages, we believe the thermal conductivity may be further enhanced. Given that electrospinning is a quick and low cost process to produce nanofibers with enhanced thermal conductivity, this study points to the potential of electrospun polymer nanofibers as materials with good thermal transport properties.

Acknowledgements

The authors thank the financial support from National Science Foundation (Grant# CMMI-1462866). Jian Ma acknowledges financial support from the National Basic

Research Program of China (2011CB707601, 2011CB707605) and the China Scholarship Council (CSC 201306090111).

References

1. Q. P. Pham, U. Sharma and A. G. Mikos, *Tissue Eng*, 2006, 12, 1197-1211.
2. J. M. Moran-Mirabal, J. D. Slinker, J. A. DeFranco, S. S. Verbridge, R. Ilic, S. Flores-Torres, H. Abruna, G. G. Malliaras and H. G. Craighead, *Nano Lett*, 2007, 7, 458-463.
3. H. Q. Liu, J. B. Edel, L. M. Bellan and H. G. Craighead, *Small*, 2006, 2, 495-499.
4. Y. Ishii, R. Kaminose and M. Fukuda, *Mater Lett*, 2013, 108, 270-272.
5. N. J. Pinto, A. T. Johnson, A. G. MacDiarmid, C. H. Mueller, N. Theofylaktos, D. C. Robinson and F. A. Miranda, *Appl Phys Lett*, 2003, 83, 4244-4246.
6. H. Q. Liu, C. H. Reccius and H. G. Craighead, *Appl Phys Lett*, 2005, 87.
7. A. Babel, D. Li, Y. N. Xia and S. A. Jenekhe, *Macromolecules*, 2005, 38, 4705-4711.
8. H. Q. Liu, J. Kameoka, D. A. Czaplewski and H. G. Craighead, *Nano Lett*, 2004, 4, 671-675.
9. P. Anzenbacher and M. A. Palacios, *Nat Chem*, 2009, 1, 80-86.
10. J. B. Ballengee and P. N. Pintauro, *Macromolecules*, 2011, 44, 7307-7314.
11. M. M. Mannarino, D. S. Liu, P. T. Hammond and G. C. Rutledge, *Acs Appl Mater Inter*, 2013, 5, 8155-8164.
12. S. S. Verbridge, J. M. Parpia, R. B. Reichenbach, L. M. Bellan and H. G. Craighead, *J Appl Phys*, 2006, 99.
13. H.-S. P. Park, Y. O. , *Korean J. Chem. Eng*, Eng. 22, 165–172 (2005).
14. Donaldson|Torit|Ultra-Web Media Technology. at <http://www2.donaldson.com/torit/en-us/pages/products/ultra-webmediatechnology.aspx>.
15. Y. J. Jung, S. Kar, S. Talapatra, C. Soldano, G. Viswanathan, X. S. Li, Z. L. Yao, F. S. Ou, A. Avadhanula, R. Vajtai, S. Curran, O. Nalamasu and P. M. Ajayan, *Nano Lett*, 2006, 6, 413-418.
16. S. Kazaoui, N. Minami, B. Nalini, Y. Kim and K. Hara, *J Appl Phys*, 2005, 98.
17. A. B. Dalton, S. Collins, E. Munoz, J. M. Razal, V. H. Ebron, J. P. Ferraris, J. N. Coleman, B. G. Kim and R. H. Baughman, *Nature*, 2003, 423, 703-703.
18. X. J. Wang, V. Ho, R. A. Segalman and D. G. Cahill, *Macromolecules*, 2013, 46, 4937-4943.
19. T. Zhang and T. F. Luo, *Acs Nano*, 2013, 7, 7592-7600.
20. A. Henry and G. Chen, *Phys Rev Lett*, 2008, 101.
21. A. Henry and G. Chen, *Phys Rev B*, 2009, 79.
22. S. Shen, A. Henry, J. Tong, R. Zheng and G. Chen, *Nat Nanotechnol*, 2010, 5, 251-255.
23. V. Singh, T. L. Bougher, A. Weathers, Y. Cai, K. Bi, M. T. Pettes, S. A. McMenamin, W. Lv, D. P. Resler, T. R. Gattuso, D. H. Altman, K. H. Sandhage, L. Shi, A. Henry and B. A. Cola, *Nat Nanotechnol*, 2014, 9, 384-390.
24. Z. Zhong, M. C. Wingert, J. Strzalka, H. H. Wang, T. Sun, J. Wang, R. Chen and Z. Jiang, *Nanoscale*, 2014, 6, 8283-8291.
25. C. Canetta, S. Guo and A. Narayanaswamy, *The Review of scientific instruments*, 2014, 85, 104901.
26. T. Yoshioka, R. Dersch, A. Greiner, M. Tsuji and A. K. Schaper, *Macromolecular Materials and Engineering*, 2010, 295, 1082-1089.
27. D. M. Rein, L. Shavit-Hadar, R. L. Khalfin, Y. Cohen, K. Shuster and E. Zussman, *Journal of Polymer Science Part B: Polymer Physics*, 2007, 45, 766-773.
28. S. R. Givens, K. H. Gardner, J. F. Rabolt and D. B. Chase, *Macromolecules*, 2007, 40, 608-610.
29. P. F. Li, L. Hu, A. J. H. McGaughey and S. Shen, *Adv Mater*, 2014, 26, 1065-1070.
30. D. Y. Li, Y. Y. Wu, P. Kim, L. Shi, P. D. Yang and A. Majumdar, *Appl Phys Lett*, 2003, 83, 2934-2936.
31. M. C. Wingert, Z. C. Y. Chen, S. Kwon, J. Xiang and R. K. Chen, *Review of Scientific Instruments*,

2012, 83.
32. A. L. Moore and L. Shi, *Meas Sci Technol*, 2011, 22.
33. J. L. Zheng, M. C. Wingert, E. Dechaumphai and R. K. Chen, *Review of Scientific Instruments*, 2013, 84.
34. G. R. Strobl and W. Hagedorn, *J Polym Sci Pol Phys*, 1978, 16, 1181-1193.
35. J. E. Lasch and S. L. Hsu, *Abstr Pap Am Chem S*, 1981, 182, 73-Poly.
36. S. L. Wunder, *Macromolecules*, 1981, 14, 1024-1030.
37. S. L. Wunder and S. D. Merajver, *J Polym Sci Pol Phys*, 1986, 24, 99-110.
38. L. H. Wang, R. S. Porter, H. D. Stidham and S. L. Hsu, *Macromolecules*, 1991, 24, 5535-5538.
39. H. Sato, M. Shimoyama, T. Kamiya, T. Amari, S. a?ic, T. Ninomiya, H. W. Siesler and Y. Ozaki, *J Appl Polym Sci*, 2002, 86, 443-448.
40. P. Taddei, M. Di Foggia and S. Affatato, *J Raman Spectrosc*, 2011, 42, 1344-1352.
41. L. M. Bellan and H. G. Craighead, *Polymer*, 2008, 49, 3125-3129.
42. J. M. Lagaron, N. M. Dixon, W. Reed, J. M. Pastor and B. J. Kip, *Polymer*, 1999, 40, 2569-2586.
43. Hassan Ebadi-Dehaghani and Monireh Nazempour (2012). Thermal Conductivity of Nanoparticles Filled Polymers, Smart Nanoparticles Technology, Dr. Abbass Hashim (Ed.), ISBN: 978-953-51-0500-8, InTech, DOI: 10.5772/33842.
44. O. Ero-Phillips, M. Jenkins and A. Stamboulis, *Polymers-Basel*, 2012, 4, 1331-1348.
45. M. Pigeon, R. E. Prudhomme and M. Pezolet, *Macromolecules*, 1991, 24, 5687-5694.
46. G. H. Kim, D. Lee, A. Shanker, L. Shao, M. S. Kwon, D. Gidley, J. Kim and K. P. Pipe, *Nat Mater*, 2015, 14, 295-300.
47. L. Kurelec, S. Rastogi, R. J. Meier and P. J. Lemstra, *Macromolecules*, 2000, 33, 5593-5601.
48. D. L. Vezie, E. L. Thomas and W. W. Adams, *Polymer*, 1995, 36, 1761-1779.

Table 1. Band assignments for Raman spectra of PE.

Frequency (cm^{-1})	Assignment	Feature
1060	Asymmetric C–C stretching	crystalline, anisotropic
1080	C–C stretching	amorphous
1130	symmetric C–C stretching	crystalline, anisotropic
1166	CH_2 rocking	crystalline
1295	CH_2 twisting	crystalline, anisotropic
1360	CH_3 wagging	amorphous
1416	CH_2 bending	crystalline
1440	CH_2 bending	anisotropic
1460	CH_2 bending	anisotropic

Captions:

Figure 1. Electrospinning PE nanofibers. (a) Schematic of PE electrospinning at elevated temperature using an IR-heating system. (b-d) A schematic model of structural changes of the PE molecules at each fabrication step. (b) PE powder with crystalline lamellae and amorphous regions in solid state. (c) Extended PE molecule chains dissolved in the solvent with random orientation. (d) During the electrospinning process, the PE molecule chains aligned into more ordered arrangement.

Figure 2. (a) A single PE nanofiber collected on PDMS membrane. (b) An SEM micrograph of a single nanofiber suspended between two adjacent SiN_x membranes on a measurement device. (c) A high magnification SEM micrograph of a PE nanofiber of 56 nm diameter. (d) An optical image of the laser focused on individual PE nanofiber for Raman measurement.

Figure 3. Raman spectra acquired at the same position on two PE nanofibers fabricated at different voltage: (a) a fiber electrospun at 15 kV, and (b) a fiber electrospun at 40 kV. These three Raman spectra essentially overlap, suggesting negligible damage due to the incident laser light.

Figure 4. Raman spectra of PE powder and PE nanofibers prepared at different voltages. As the electrospinning voltage increases, the band at 1130 cm^{-1} enhances while the band at 1060 cm^{-1} decreases. The intensity ratio of the 1130 and 1060 cm^{-1} bands is an indicator of the molecular orientation in PE. Additionally, the band at 1416 cm^{-1} (assigned to orthorhombic crystallinity) becomes stronger as the electrospinning voltage increases.

Figure 5. Thermal conductivity and structure of PE nanofibers. (a) Room-temperature thermal conductivities of the fibers, which increases as the electrospinning voltage gets larger. (b) The intensity ratio of the 1130 and 1060 cm^{-1} bands, which reflects the molecular orientation in PE. This ratio increases with the electrospinning voltage, indicating a better molecular orientation. (c) Temperature dependence of the thermal conductivity. The uncertainty of the measurement mainly comes from the fiber dimension characterization. (d) The fraction of orthorhombic phase is proportional to the band area ratio $I_{1416}/I_{1295+1305}$, which gets larges with the electrospinning voltage.

Figure 6. (a) The thermal conductivity of four PE nanofibers of different diameter electrospun at the same voltage (45 kV). (b) Comparison of our thermal conductivity data with published values for PE.

Figure 7. The effects of electron beam irradiation. (a) An SEM micrograph of the initial fiber. (b) An SEM micrograph of the irradiated fiber. It is clear that the length of the PE fiber has decreased after electron beam irradiation. (c) The thermal conductivity of a nanofiber before and after SEM characterization. The electron beam altered the microstructure of the nanofiber, resulting in a reduction of thermal conductivity. (d) Micro-Raman spectra of a same PE nanofiber before and after SEM irradiation, indicating significant structural change upon SEM irradiation.

Figure 8. Raman spectra of PE with solvent trapped inside. (a) Raman spectra of PE fibers electrospun at various voltages with 18G needle and 500 μl/min solution flow rate. As the voltage increases, more solvent appears to be trapped in the fibers. (b) Raman spectra of a PE fiber before and after overnight storage under vacuum. It is clear that the peaks due to trapped solvent disappear after this overnight process.

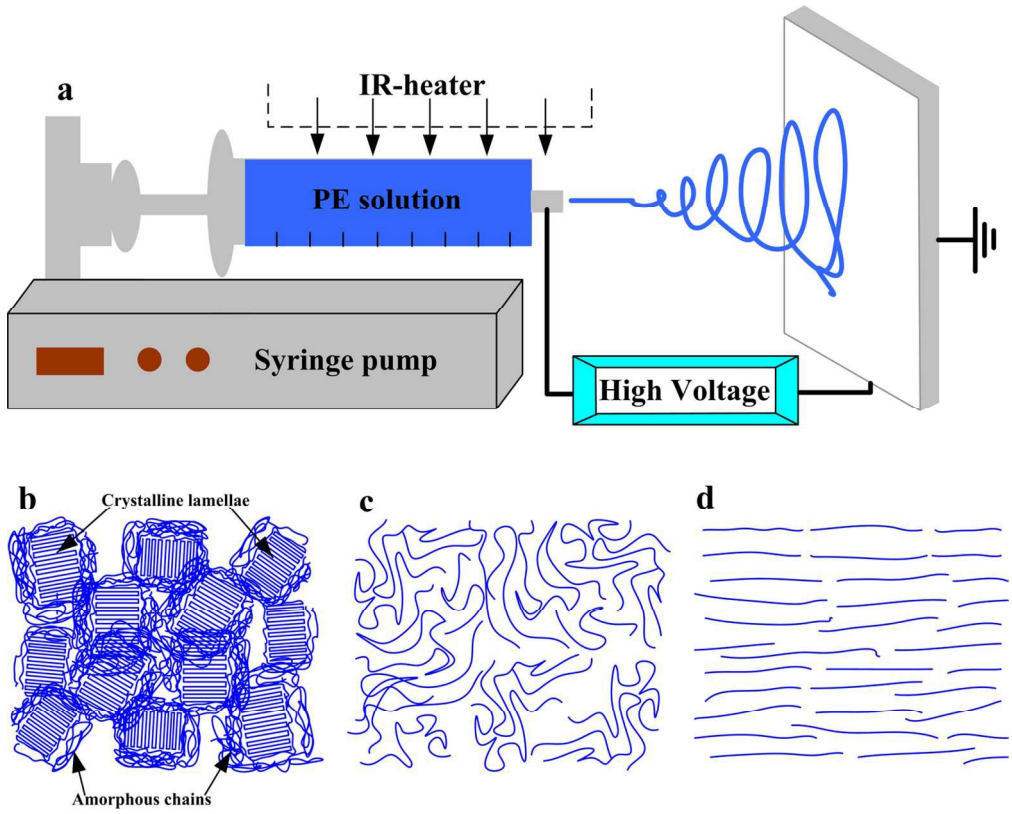

137x110mm (300 x 300 DPI)

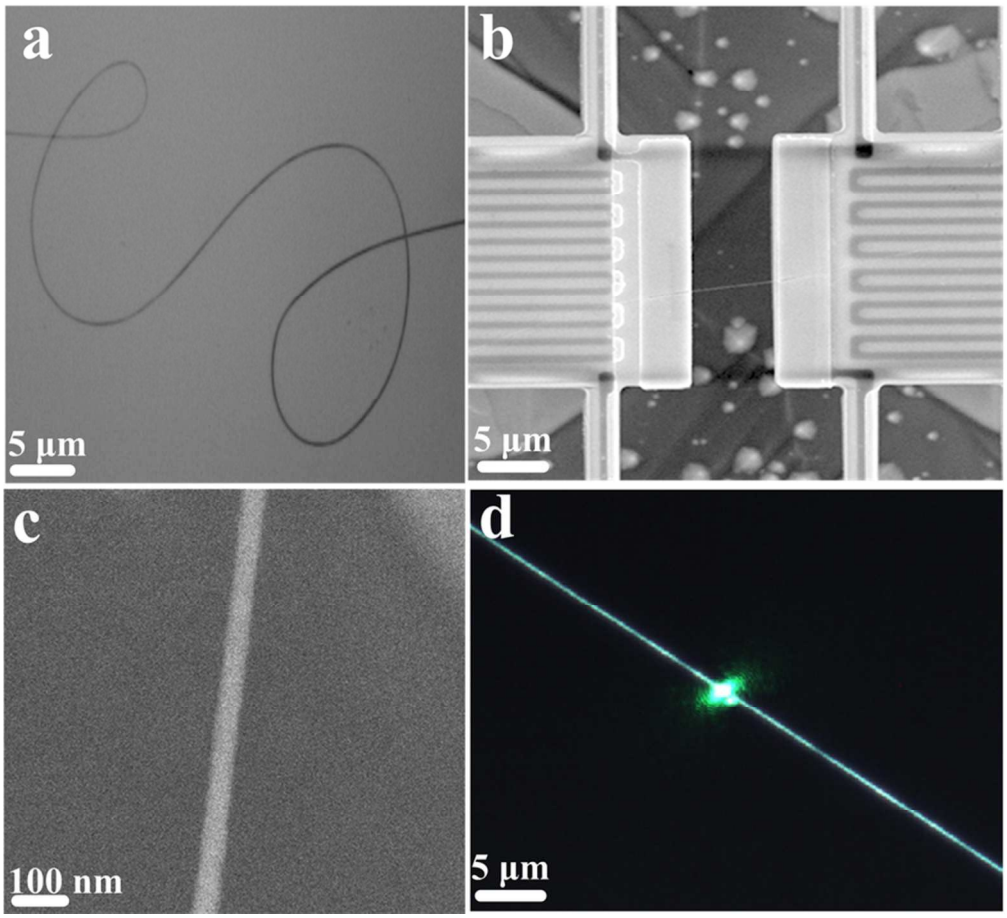

76x71mm (300 x 300 DPI)

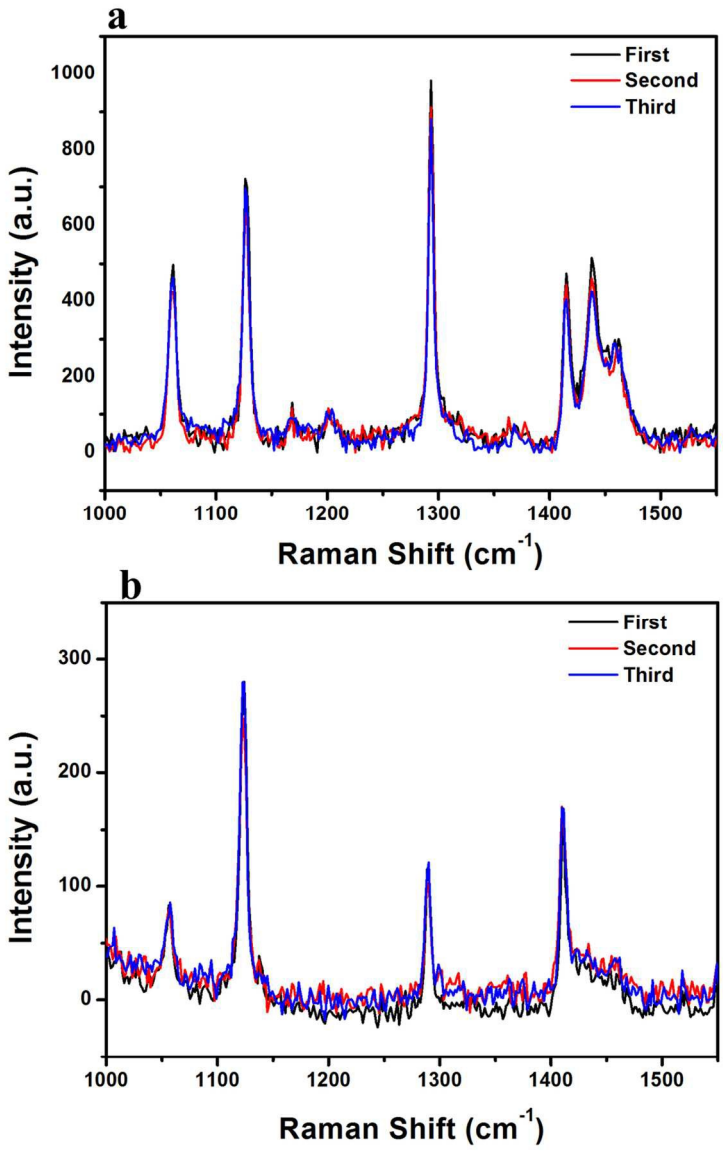

110x147mm (300 x 300 DPI)

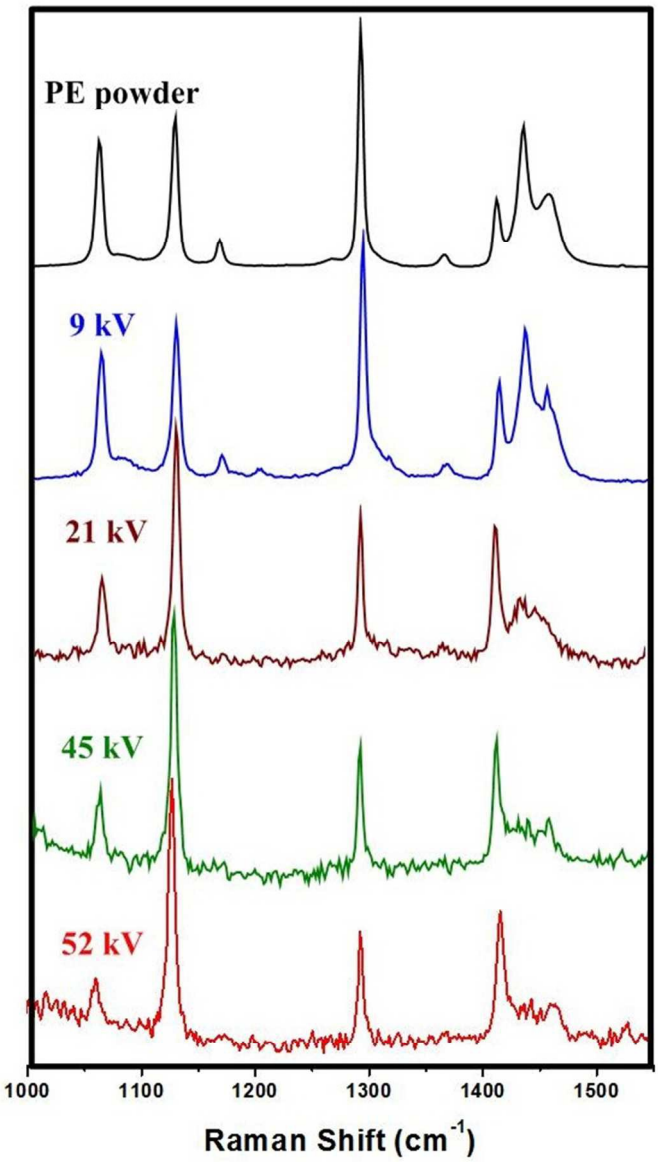

135x221mm (300 x 300 DPI)

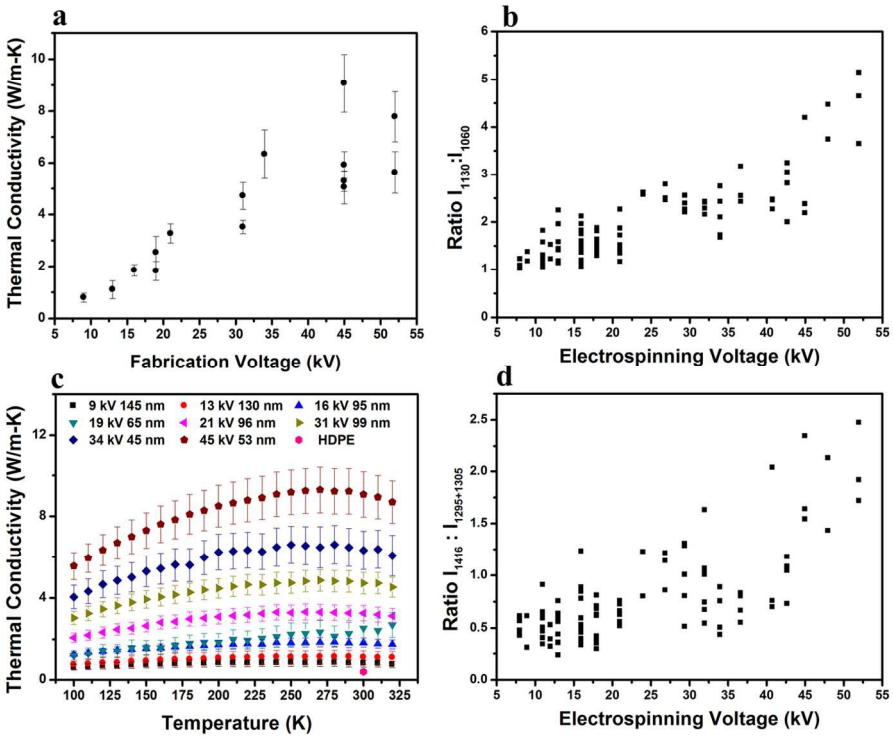

130x99mm (300 x 300 DPI)

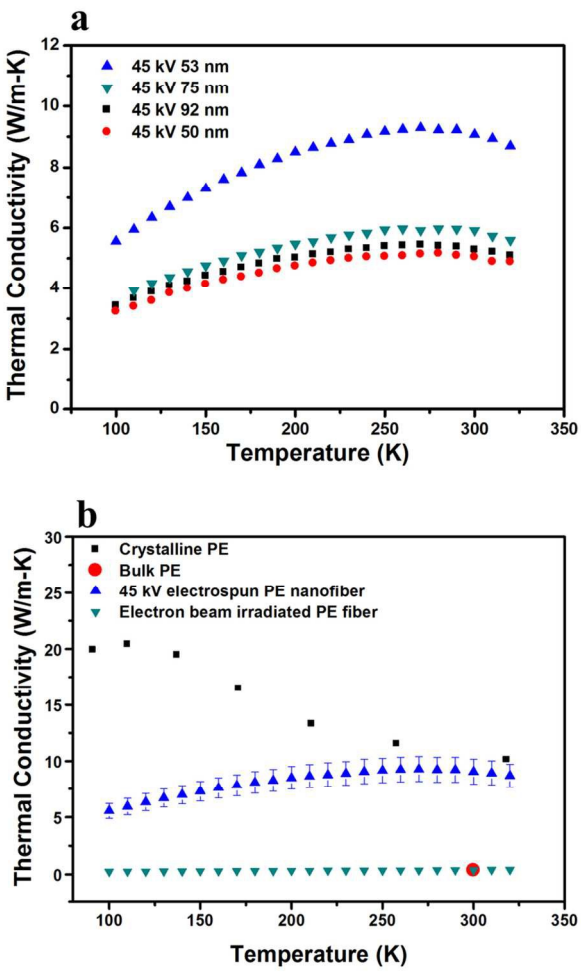

114x114mm (300 x 300 DPI)

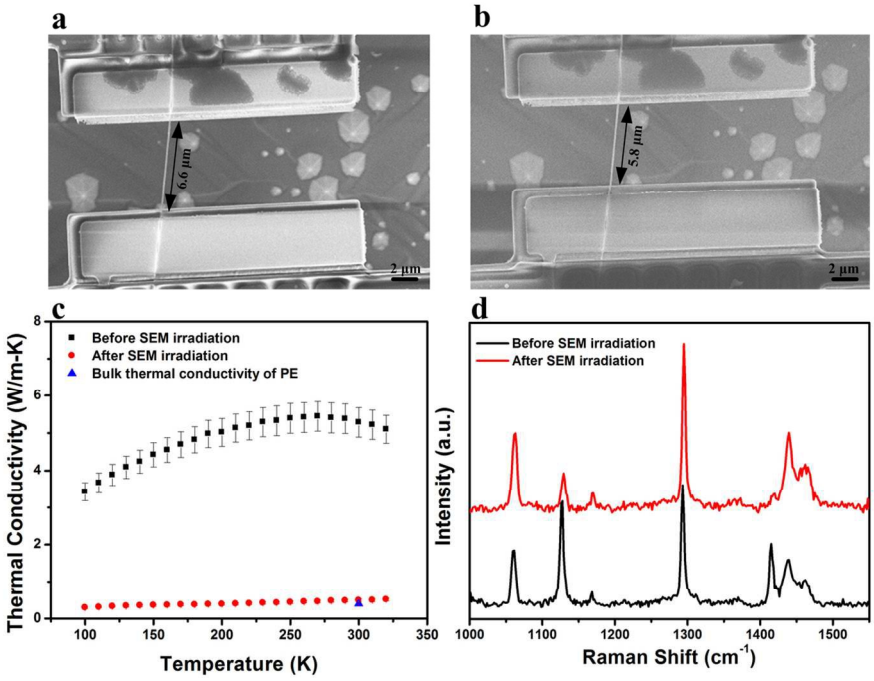

119x83mm (300 x 300 DPI)

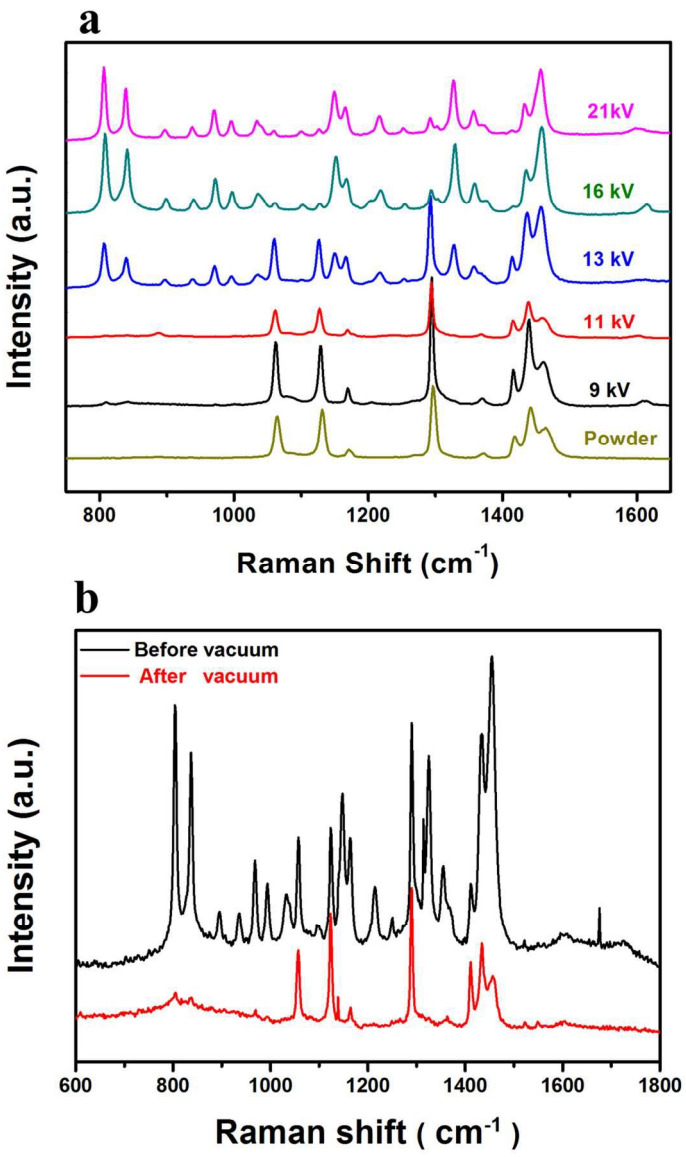

112x151mm (300 x 300 DPI)